

Search for Diffuse X-rays from the Bow Shock Region of Runaway Star BD+43°3654 with Suzaku

Yukikatsu TERADA¹ Makoto S. TASHIRO¹ Aya BAMBA² Ryo YAMAZAKI² Tomomi KOUZU¹ Shu KOYAMA¹ and
Hiromi SETA³

¹Graduate School of Science and Engineering, Saitama University, 255 Simo-Ohkubo, Sakura-ku, Saitama City, Saitama
338-8570, Japan

terada@phy.saitama-u.ac.jp

²Department of Physics and Mathematics, College of Science and Engineering, Aoyama Gakuin University, 5-10-1 Fuchinobe,
Chuo-ku, Sagami-hara, Kanagawa 252-5258, Japan

³Department of Physics, Science, Rikkyo University, 3-34-1, Nishi-Ikebukuro, Toshima-ku, Tokyo, Japan

(Received 2012 June 5; accepted 2012 July 23)

Abstract

The bow shocks of runaway stars with strong stellar winds of over 2000 km s⁻¹ can serve as particle acceleration sites. The conversion from stellar wind luminosity into particle acceleration power has an efficiency of the same order of magnitude as those in supernova remnants, based on the radio emission from the bow shock region of runaway star BD+43°3654 (Benaglia et al. 2010). If this object exhibits typical characteristics, then runaway star systems can contribute a non-negligible fraction of Galactic cosmic-ray electrons. To constrain the maximum energy of accelerated particles from measurements of possible non-thermal emissions in the X-ray band, Suzaku observed BD+43°3654 in April 2011 with an exposure of 99 ks. Because the onboard instruments have a stable and low background level, Suzaku detected a possible enhancement over the background of 7.6 ± 3.4 cnt arcmin⁻² at the bow shock region, where the error represents the 3 sigma statistics only. However, the excess is not significant within the systematic errors of non-X-ray and cosmic-ray backgrounds of the X-ray Imaging Spectrometer, which are ± 6.0 and ± 34 cnt arcmin⁻², respectively, and the 3-sigma upper limit in the X-ray luminosity from the shock region, which is 1.1×10^{32} erg s⁻¹ per 41.2 arcmin² in the 0.5 to 10 keV band. This result leads to three conclusions: (1) a shock-heating process is inefficient on this system; (2) the maximum energy of electrons does not exceed ~ 10 TeV, corresponding to a Lorentz factor of less than 10⁷; and (3) the magnetic field in the shock acceleration site might not be as turbulent as those in pulsar wind nebulae and supernova remnants.

Key words: acceleration of particles — X-rays: stars — stars: early-type — stars: individual (BD+43°3654)

1. Introduction

1.1. Runaway stars as particle acceleration sites

An important goal of astrophysics is to understand the non-thermal phenomena in the universe. In our galaxy, pulsars and X-ray binaries are well-known objects that generate high-energy electrons and possibly protons, which emit non-thermal photons (e.g., Sturrock 1971; Ruderman & Sutherland 1975; Cheng et al. 1986a; Cheng et al. 1986b; Harding & Gaisser 1990). Recently, sensitive searches of non-thermal X-rays have led to magnetic white dwarfs also being considered as possible non-thermal emitters (Terada et al. 2008b; Terada et al. 2010; Terada & Dotani 2011). In addition to rotating magnetospheres, like pulsars, shocks in supernova remnants (SNRs) and pulsar wind nebulae (PWNe) are the most common Galactic cosmic-ray acceleration sites (e.g., Shklovskii 1953; Ginzburg 1953; Bell 1978; Lagage & Cesarsky 1983; Kennel & Coroniti 1984; Koyama et al. 1995; Rees & Gunn 1974). Searching for new types of particle-acceleration sites is a possible key to understand-

ing the non-thermal universe.

In this paper, we focus on early-type massive stars with velocities greater than 30 km s⁻¹, that is, runaway OB stars, as another source of non-thermal emission. The most prominent characteristics of runaway OB stars are their high spatial velocities and their very fast stellar winds. The velocities of the stellar winds reach a few thousand kilometers per second, which is comparable with the shock speeds of young SNRs (Bamba et al. 2005 and references therein). Thus, in the rest frame of an OB star, two shocks (a bow shock and a wind termination shock) and a contact discontinuity appear in order to balance the ram pressure of the interstellar gas with that of the stellar wind (del Valle & Romero 2012). Bow shock structures can often be seen in infrared images of runaway OB stars (van Buren & McCray 1988; Peri et al. 2012). Benaglia et al. (2010) have reported radio observations in the NRAO-VLA Sky Survey program, indicating the presence of high-energy electrons in the bow shock region of runaway star BD+43°3654.

The object BD+43°3654 is thought to be a blue strag-

gler system formed by a close encounter between two tight massive binaries (Gvaramadze & Bomans 2008) in the core of the Cygnus OB2 association (Comerón et al. 2002 and references therein), which is the most massive OB association in the solar neighborhood, at a distance of $d = 1.4$ kpc (Hanson 2003; Comerón & Pasquali 2007). The spectral type of the star is O4If with an age of about 1.6 Myr and a stellar mass of $70 \pm 15 M_{\odot}$ (Comerón & Pasquali 2007); the star is one of the most massive runaway stars known today. The heliocentric radial velocity is measured to be $v_{\star} = -66.2 \pm 9.4$ km s $^{-1}$ (Kobulnicky et al. 2010). The typical mass-loss rate for O4I stars with a stellar wind velocity of $v_{\text{sw}} = 2300$ km s $^{-1}$ is $\dot{M} = 10^{-5} M_{\odot} \text{ yr}^{-1}$ (Markova et al. 2004; Repolust et al. 2004). The bow shock structure was found by IRAS observations in a systematic 60 μm survey (van Buren & McCray 1988), and was confirmed by the Midcourse Space eXperiment in the D and E bands (Comerón & Pasquali 2007). Synchrotron emission was also found from this region in the radio bands at 1.42 GHz and 4.86 GHz, as already mentioned (Benaglia et al. 2010).

1.2. Similarity with SNR cases

We can investigate the runaway system as a shock acceleration site by using its similarities with SNRs: velocity of stellar wind, system size, environment of inter-stellar matter, etc. If we adopt the typical parameters of stellar winds from O4I stars (Markova et al. 2004; Repolust et al. 2004), the stellar wind has a kinetic luminosity up to

$$\begin{aligned} \dot{E}_{\text{sw}} &= 2 \times 10^{37} \left(\frac{\dot{M}}{10^{-5} M_{\odot} \text{ yr}^{-1}} \right) \\ &\times \left(\frac{v_{\text{sw}}}{2300 \text{ km s}^{-1}} \right)^2 \text{ erg s}^{-1}. \end{aligned} \quad (1)$$

The termination shock causes particle acceleration which generates high-energy protons and electrons (del Valle & Romero 2012). In order to account for the radio luminosity of BD+43°3654 reported by Benaglia et al. (2010), high energy electrons with the energy index of $p \sim 2.0$ should have a total energy of $E_e \sim 2 \times 10^{45}$ ergs, under the assumption of equipartition between the energy densities of electrons u_e and magnetic field u_B , as is the case with many young SNRs (Bamba et al. 2003; Bamba et al. 2005). In this case, corresponding magnetic-field strength B is about a few tens of micro Gauss. Then, the cooling timescale of electrons emitting synchrotron radiation with characteristic frequency ν (Reynolds & Keohane 1999),

$$\tau_{\text{sync}} \sim 10^{15} \left(\frac{B}{10 \mu\text{G}} \right)^{-3/2} \left(\frac{\nu}{1 \text{ GHz}} \right)^{-1/2} \text{ s}, \quad (2)$$

is much longer than the dynamical timescale,

$$\tau_{\text{dy}} \sim \frac{R_0}{v_{\text{sw}}} = 3 \times 10^{10} \text{ s}, \quad (3)$$

where $R_0 \sim 2$ pc is the distance to the shock front of the bow shock measured by Benaglia et al. (2010).

Electrons are accelerated and emitting synchrotron radiation around the shock region. They escape from the

shock region flowing out along the stream backward of the star in a certain time scale. Assuming that the system is in a steady state, the electron production rate L_e is roughly identical to the loss rate from the system. In that case, L_e will be described by E_e divided by the escaping time scale. Here, we regard the dynamical effects should be dominant, since the cooling time scale of the electrons is fairly longer than the dynamical time scale, τ_{dy} , as described above (equations (2) and (3)). Thus a rough estimate of L_e is $\sim E_e/\tau_{\text{dy}} = 6 \times 10^{34}$ erg s $^{-1}$, which corresponds to about 0.3% of \dot{E}_{sw} given in equation (1). Therefore, the conversion from the energies of stellar winds into the acceleration power of particles in this runaway star system has an efficiency of the same order of magnitude as those in SNRs.

Since about 10% of O-stars exhibit bow shock structures (Peri et al 2012), the $\sim 2,000$ runaway stars in our Galaxy can produce a non-negligible proportion of about 10% of the cosmic-ray electrons observed at Earth (i.e., 10^{38} erg s $^{-1}$), if BD+43°3654, with its high-energy electron production rate of 6×10^{34} erg s $^{-1}$, represents the typical case of a runaway-star system as a particle acceleration site. Therefore, it is important to study physical parameters of the particle acceleration process in BD+43°3654.

In the sense of energetics, BD+43°3654 is an SNR-equivalent particle acceleration site. Then, the next studies should be how much energy the particles gain in the system. The maximum energy of accelerated electrons, E_{max} , is measured by the roll-off frequency, ν_{roll} , of the synchrotron radiation. If E_{max} is $\sim 8\text{--}20$ TeV as suggested by Benaglia et al. (2010), then, according to equation (2) in Reynolds & Keohane (1999), ν_{roll} should be $\sim 10^{16\text{--}20}$ Hz, which comes into the X-ray band. If the spectrum were simply extended from the radio band so that $\nu_{\text{roll}} = \infty$, then X-rays should be clearly detected with the sensitivities of current missions. In that case the absence of X-rays would provide a unique upper limit E_{max} . However, high sensitivity to diffuse X-ray emissions is required in this case. In this study, we performed an X-ray search for possible synchrotron emission from the shock region of BD+43°3654 with the X-ray satellite Suzaku (Mitsuda et al. 2007).

The rest of this paper is organized as follows. We describe the X-ray observations of this object in Section 2, summarize the results of Suzaku analyses in Section 3, and discuss our results in Section 4.

2. Observation and Data Reduction

2.1. Suzaku observation of BD+43°3654

Suzaku is the fifth in a series of Japanese X-ray satellites having sensitivities in the 0.2–600 keV band (Mitsuda et al. 2007). It carries two X-ray instruments on board: the X-ray Imaging Spectrometer (XIS) for the 0.2–12 keV band (Koyama et al. 2007), and the Hard X-ray Detector (HXD) for the 12–600 keV band (Takahashi et al. 2007). Although both instruments have very low-background signals (Tawa et al. 2008; Fukazawa et al. 2009), which enable us to perform high sensitivity surveys of X-rays, the

Suzaku XIS is most suitable for our purpose because it is capable of imaging and stable backgrounds.

We observed BD+43°3654 and the bow shock region with Suzaku from 2011 April 4 1:53 UT to April 6 2:13 UT (OBSID=506004010). To put the bow shock region at the XIS nominal pointing position, the aiming point was set to $(\alpha, \delta)[J2000] = (20^{\text{h}}33^{\text{m}}40.00^{\text{s}}, +44^{\circ}03'00.0'')$, although the runaway star is at $(\alpha, \delta)[J2000] = (20^{\text{h}}33^{\text{m}}36.077^{\text{s}}, +43^{\circ}59'07.40'')$. The XIS was operated in the normal clocking mode, without window/burst options but with the Space Charge-Injection (SCI) function (Nakajima et al. 2008). The XIS consists of three front-side illuminated (FI) CCD chips (XIS0, XIS2, and XIS3) and one back-side illuminated (BI) chip (XIS1). XIS2 was not operational due to damage from a meteoroid strike. HXD was operated in nominal mode: half of the 64 PIN diodes were operated with a voltage of 400 V and the others at 500 V, and the PMTs were operated at nominal gain.

2.2. Data reduction

We used the observation datasets processed by the standard Suzaku pipeline version 2.5.16.29, with the calibration version (CALDBVER) of `hxd20101202`, `xis20101108`, `xrt20100730`, and `xrs20060410`. We used `ftools` from the HEADAS 6.11 package with XSPEC version 12.7.0.

The source was detected by the XIS in the 0.5–10 keV band at an average count rate of 0.15 and 0.28 cnt s^{-1} per sensor in the FI- and BI- CCD cameras, respectively. Cleaned events of the XIS data were obtained using the standard criteria of the pipeline process. The total exposure of the XIS was 99.0 ks.

We did not use the HXD-GSO data because of sensitivity limitations. According to the INTEGRAL catalog, there were no contaminating sources in the field of view (FOV) of the HXD-PIN detector. The cleaned events from HXD-PIN were obtained by using the standard criteria of the process. The total exposure of HXD-PIN was 82.5 ks. The averaged count rate of the cleaned PIN data including backgrounds was 0.40 cnt s^{-1} in the 13–70 keV band. The non-X-ray background (NXB) events were estimated and provided by the HXD team. We used them with `METHOD='LCFITDT(bgd_d)'` and the `METHODV='2.0over804'`. The average count rate of the NXB was 0.38 cnt s^{-1} in the same energy range, and the residual count rate is consistent with the level of the cosmic X-ray background (CXB, 0.02 cnt s^{-1}) within the systematic errors of NXB (Fukazawa et al. 2009). Therefore, HXD-PIN detected no significant signals in the 13–70 keV band, and thus we do not use the HXD data in the following analyses.

3. Analyses and Results

3.1. X-ray sources in the field of view

We first checked the XIS images in the 0.5–10 keV band. The spatial distributions of the non X-ray backgrounds (NXBs) on the XIS chips in the 0.5–10 keV band were estimated by the Suzaku `ftool xisnabgen` (Tawa et al. 2008) using the background database in the CALDB area for

the period from 120 days before to 30 days after the observation. After the subtraction of the NXB image from the sky image with the XIS in the same energy bandpass, the vignetting effects of the X-ray telescopes (XRTs) were corrected by a simulated map calculated for a uniform sky input with the ray-tracing tool `xissim` (Ishisaki 2007). In this simulation, we assume that the energy spectrum of incident photons follows the power-law shape with a photon index of 1.0. Changes of ± 1.0 in the photon index correspond to changes in image shapes at the $\pm 5\%$ level. The vignetting-corrected X-ray image from the XIS in the 0.5–10 keV band is shown in Fig. 1.

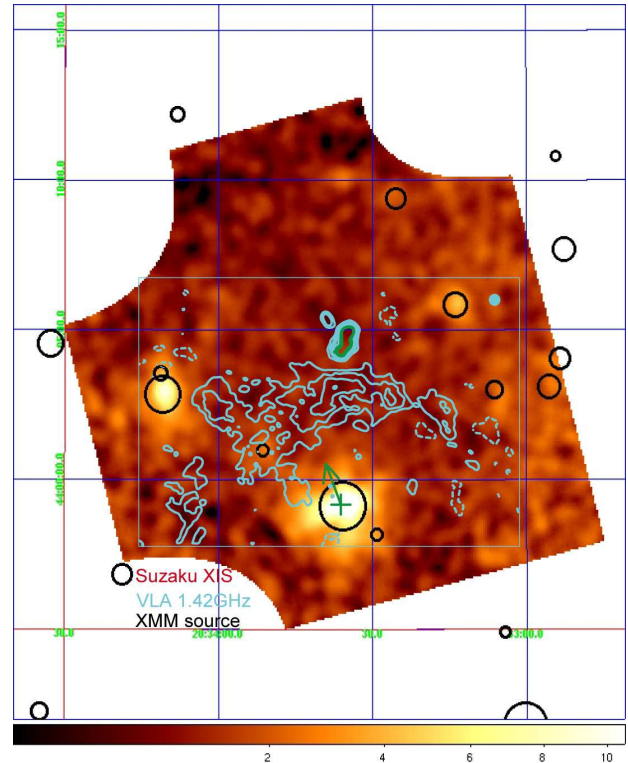


Fig. 1. The color map shows the X-ray image of BD+43°3654 with the Suzaku XIS in the 0.5–10 keV band. The areas irradiated by the calibration sources of ^{55}Fe are excluded from the image. The radio image in the 1.42 GHz band obtained by the VLA observation (Benaglia et al. 2010) is overlaid as the contour image in cyan; the radio data is valid in the cyan box. The black circles represent point sources detected by *XMM-Newton*, which are listed in Table 1. The position and runaway direction of BD+43°3654 are also shown in green with the cross and arrow, respectively.

It is important in diffuse X-ray observations to extract (or to estimate the flux of) dim point sources in the field of view, to reduce systematic errors caused by fluctuations of unresolved sources in CXB. The brightest source is BD+43°3654 itself; the X-ray image around the object was consistent with the point-spread function of the XRTs. In the X-ray light curve, after barycentric correction by *aebarycen* (Terada et al. 2008a), we found neither significant flares nor coherent-periodic signals in the 16 to 10,000 s range. The X-ray spectrum was well described by a MEKAL model (Mewe et al. 1985; Liedahl

et al. 1995; Kaastra et al. 1996) with a temperature of $0.60^{+0.14}_{-0.09}$ keV and a metal abundance of $0.32^{+0.40}_{-0.17}$ solar, where the photoabsorption of the hydrogen column density was $N_{\text{H}} = 1.45^{+0.26}_{-0.17} \times 10^{22} \text{ cm}^2$. The emission measure and X-ray luminosity in the 0.5–10 keV band were $\text{EM} = 6.5^{+9.9}_{-2.8} \times 10^{55} \text{ cm}^{-3}$ and $3.7^{+5.6}_{-1.6} \times 10^{31} \text{ erg s}^{-1}$, respectively. The value of N_{H} is consistent with the galactic neutral hydrogen map by Kalberla et al. (2005), and other parameters were well understood as being typical of X-ray emissions from O-type stars (Nazé et al. 2011), following the rough relation between kT (keV) and EM (cm^{-3}) given by $\log \text{EM} \sim 53.9 - \log kT$.

For the further rejection of contaminating sources, we checked the archive data of BD+43°3654 from *XMM-Newton* (OBSID = 0653690101, PI= Zabalza Victor, starting from 2010 May 8 08:04 UT, 46.7 ks exposure). Several faint point sources that contaminate the FOV of the XIS are listed in table 1 and are plotted as black circles in Fig. 1. Therefore, in the following analyses, we can exclude contamination by point sources with X-ray fluxes above $S_c = 3.7 \times 10^{-14} \text{ erg s}^{-1} \text{ cm}^{-2}$ in the 0.5–10 keV band.

Table 1. Point sources detected with EPIC during the *XMM-Newton* observation of OBSID= 0653690101 (except for BD+43°3654). The X-ray flux is in units of $10^{-13} \text{ erg s}^{-1} \text{ cm}^{-2}$ in the 0.5 to 10 keV band.

RA	DEC	flux
308.5455	44.047592	1.2
308.54706	44.058725	0.47
308.23159	44.051389	0.77
308.5781	43.947109	0.63
308.22298	44.067196	0.70
308.3077	44.097479	0.83
308.27586	44.050153	0.53
308.37145	43.969254	0.40
308.3562	44.156242	0.67
308.46396	44.016647	0.37

3.2. Upper limit of the X-ray flux from the bow shock region

To estimate the possible diffuse-X-ray emissions around the bow shock region numerically, we first defined three regions: ‘BD43’, ‘BSK’, and ‘BGD’, representing BD+43°3654, its bow shock, and the background areas, respectively. The definitions of these areas are shown in Fig. 2. The circular areas around the XMM sources are excluded from the BSK and BGD regions; the radii of these excluded regions were defined by their luminosities. The geometrical areas of BD43, BSK, and BGD were 11.5, 41.2, and 44.8 arcmin^2 , respectively. Then, we counted X-ray events detected with the XIS, taking into account vignetting effects of the XRTs, we obtained 288.1 ± 11.9 , 81.6 ± 2.6 , and $74.0 \pm 2.3 \text{ cnt arcmin}^{-2}$, for BD43, BSK, and BGD, respectively, where the errors are the 99% statistical ones. Thus, the events in the BSK region exceed

those in the BGD region by $7.6 \pm 3.4 \text{ cnt arcmin}^{-2}$ statistically.

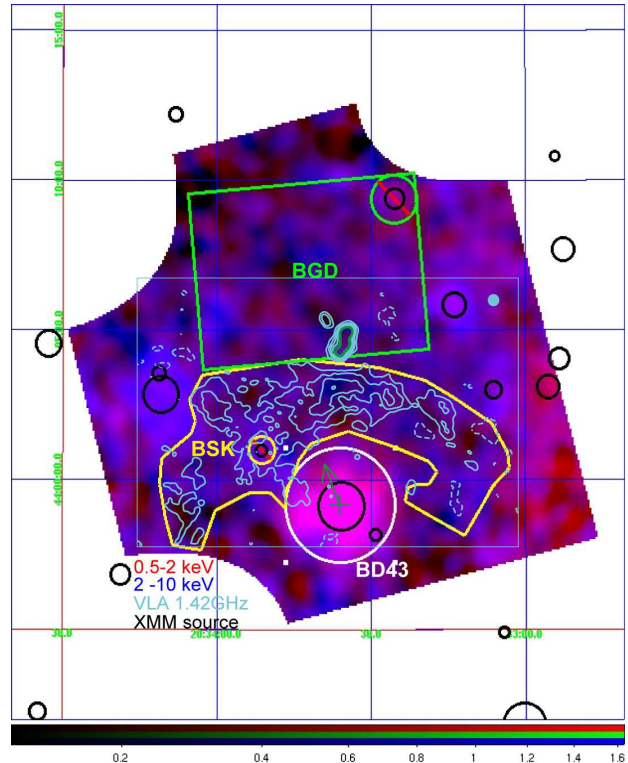


Fig. 2. The energy resolved X-ray images from the Suzaku XIS. The 0.5–2 keV and 2–10 keV images are shown in red and blue, respectively. Point sources from *XMM-Newton* are plotted as black circles, and the radio contour in the 1.42 GHz band (Benaglia et al. 2010) is displayed in cyan. The definitions of regions, BGD, BSK, and BD43, are outlined in green, yellow, and white, respectively.

The measurement of the enhanced counts in the BSK region ($7.6 \pm 3.4 \text{ cnt arcmin}^{-2}$) has systematic errors in estimations of the NXB and CXB. That of NXB is reported as 5% by Tawa et al. (2008), and we adopt this value in this paper. The systematic error in the CXB level is caused by fluctuations in numbers of unresolved point sources (which are mainly active galactic nuclei). According to the systematic studies of CXB with ASCA by Kushino et al. (2002), the CXB flux within the field of view of the GIS (Gas Imaging Spectrometer; Ohashi et al. 1996; 0.5 deg^2) fluctuated by 6.5% in the 2 to 10 keV band. Since the size of the BSK region is about 42 arcmin^2 , the fluctuation would be 43% for the BSK region by the XIS. As described in session 3.1, we removed dimmer point sources from the XIS data than the GIS observation; i.e., the flux limit for the GIS was $S_c = 2 \times 10^{-13} \text{ erg s}^{-1} \text{ cm}^{-2}$ (Kushino et al. 2002), whereas our analyses achieved $4 \times 10^{-14} \text{ erg s}^{-1} \text{ cm}^{-2}$ (section 3.1). If we adopt the index of the $\log N - \log S$ relation for the population of point sources in CXB is 1.5, the CXB flux in our observation should have 12% fluctuation after removal of point sources with *XMM-Newton*. Therefore, the systematic errors of NXB and CXB are 5% and 12% for this

FOV, respectively. Numerically, the systematic errors for the NXB and CXB in the count rates of BD43, BSK, and BGD were $\pm 1.89 \pm 20.3$, $\pm 1.91 \pm 19.2$, and $\pm 5.69 \pm 27.8$ cnt arcmin $^{-2}$, respectively. Thus, the enhancement was $7.6 \pm 3.4 \pm 6.0 \pm 34$ cnt arcmin $^{-2}$, where the first, second, third errors represent statistics, systematics in the NXB estimation, and systematics in the CXB estimation, respectively; i.e., the X-ray count rate in the BSK region is consistent with that in the BGD region within the systematic errors.

The X-ray spectrum of the BSK region, in which the vignetting-corrected CXB and the NXB were subtracted, can be well reproduced by a power-law model with a photon index of $1.10_{-0.33-0.03}^{+0.37+0.18}$ and an X-ray flux of $2.56_{-0.74-0.59}^{+0.83+0.70} \times 10^{-13}$ erg s $^{-1}$ cm $^{-2}$ in the 0.5–10 keV band, where the first and second errors, respectively, correspond to the statistical error and the combined systematic errors for CXB and NXB, at the 3 sigma level. Thus, the 3-sigma upper limit of the X-ray luminosity from the BSK region in the 0.5–10 keV band is 1.1×10^{32} erg s $^{-1}$ at a distance of 1.4 kpc.

4. Discussion

We searched for diffuse X-ray emissions from the shock region of BD+43°3654 with Suzaku (see Section 2), and found an upper limit for the diffuse X-ray luminosity of 1.1×10^{32} erg s $^{-1}$ per 41.2 arcmin 2 in the 0.5–10 keV band (see Section 3.2). By analogy with SNR systems (see Section 1.2), if the termination shock occurs in the region, interstellar materials would be shock-heated, and electrons or protons would be shock-accelerated. We discuss the efficiency of the heating by shock in Section 4.1, and the acceleration process in Section 4.2.

4.1. Efficiency of thermalization by the shock

If we assume that the value of v_{sw} for the object is the typical value of 2300 km s $^{-1}$ (Markova et al. 2004; Repolust et al. 2004) and that the stellar gas has a typical temperature of $T_{\text{is}} \sim 10^5$ K and acts as an ideal gas having a heating ratio of $\gamma = \frac{5}{3}$, then the sound speed in the gas is $c_s = 4 \times 10^6 \left(\frac{T_{\text{is}}}{10^5 \text{K}}\right)^{0.5} \left(\frac{\gamma}{5/3}\right)^{0.5}$ cm s $^{-1}$. This value is much lower than v_{sw} . Therefore, we can expect a strong termination shock to occur inside the contact discontinuity facing the runaway star, while the bow shock occurs on the opposite side. In this situation, the cold materials of the stellar wind could be shock-heated to a temperature of

$$\begin{aligned} kT^{\text{sh}} &= \frac{3}{16} \frac{\mu m_{\text{H}}}{k} \left(\frac{4v_{\text{sw}}}{3}\right)^2 \\ &= 11.2 \left(\frac{\mu}{0.615}\right) \left(\frac{v_{\text{sw}}}{2300 \text{ km s}^{-1}}\right)^2 \text{ keV}, \end{aligned} \quad (4)$$

where μ , m_{H} , and k are the mean ratio of numbers of electrons and nucleons, the mass of hydrogen, and Boltzmann constant, respectively. In other words, we can expect hot plasmas to exist immediately behind the termination

shock.

In the rest frame of the star, the interstellar-matter (ISM) gas flows toward the star and forms shocks through interaction with the stellar wind. The incoming energy of the ISM flow per unit time is $(\rho_{\text{ISM}} v_0^3 / 2) \times (4\pi R_0^2)$, where we have neglected enthalpy, and v_0 is the stellar bulk speed through the ISM. This gives a smaller contribution to the energy source of a possible thermal emission than the ejected kinetic luminosity of the stellar wind, $\dot{E}_{\text{sw}} \sim (1/2) \dot{M} v_{\text{sw}}^2 \sim 2\pi \rho v_{\text{sw}}^3 R_0^2$, by a factor of $F = v_{\text{sw}} / v_0 \sim 40$, assuming $v_0 \sim v_*$. Here, ρ_{ISM} and ρ are the densities of uniform ISM and the stellar wind just in front of the termination shock, respectively, and we simply assume the pressure balance, $\rho_{\text{ISM}} v_0^2 \sim \rho v_{\text{sw}}^2$, and a spherical shape for the termination shock with radius R_0 . However, the shocked, hot region is compressed to have a density $F^2 \rho \sim 1.6 \times 10^3 \rho$ at most, and thus we can expect an anisotropy of the emission from hot plasmas: it should be brighter toward the runaway direction as in the radio synchrotron image (Benaglia et al. 2010).

The Suzaku observation represents the upper limit of the X-ray luminosity at $< 1.1 \times 10^{32}$ erg s $^{-1}$, which corresponds to the emission measure EM of $< 3.8 \times 10^{54}$ cm $^{-3}$ for plasmas with the temperature of $kT = 11.2$ keV as expected by equation (4). This value of the upper limit of EM reduces only by factor 4 even if we change kT by one order of magnitude lower. The EM can be described as $\text{EM} = \int n_{\text{e,th}}^2 dV = \bar{n}_{\text{e,th}}^2 V_{\text{BS}} \eta$, where $n_{\text{e,th}}$ is the density of thermal electrons, V is the volume of the plasma, $\bar{n}_{\text{e,th}}$ is the averaged value of electron density, V_{BS} is the volume of the bow shock region (1.5×10^{56} cm 3 ; Benaglia et al. 2010), and η is a density-weighted filling factor of the plasma in the bow shock region. If we adopt the density of cold electrons $n_{\text{e,cl}} \sim 6$ cm $^{-3}$ (Comerón & Pasquali 2007), the upper limit of EM can be written into the following constraint;

$$\left(\frac{\bar{n}_{\text{e,th}}}{n_{\text{e,cl}}}\right)^2 \eta < 0.7 \times 10^{-3}. \quad (5)$$

Therefore, the shock-heating process is inefficient in the shock region of the runaway star BD+43°3654. If all the cold materials are heated into the hot plasma ($n_{\text{e,th}} = n_{\text{e,cl}}$), for example, then a very small fraction of the shock region would be shock-heated; i.e., when a top thin region emits thermal X-rays as discussed in del Valle & Romero (2012), the thickness of the region would be less than 2×10^{15} cm. Otherwise, if the all the shock region emit thermal X-rays ($\eta = 1$), then only $\left(\frac{\bar{n}_{\text{e,th}}}{n_{\text{e,cl}}}\right) \sim 3\%$ of cold electrons are heated by shocks. We expect further deep survey by a micro-calorimeter onboard the near future X-ray mission, ASTRO-H.

4.2. Constraints on a possible particle acceleration process by stellar winds

As indicated by Benaglia et al. (2010), high-energy electrons with $p \sim 2.0$ on average should exist around the shocked region and emit synchrotron radio radiation. From the X-ray observations obtained with Suzaku, we

obtained a 3-sigma upper-limit of the X-ray luminosity at 1.1×10^{32} erg s⁻¹ in the 0.5 to 10 keV band. Fig. 3 shows the multi-wavelength spectra from the shocked region of BD+43°3654. We have also plotted the energy spectra of synchrotron emissions for $p = 2.5$ or 2.0 , assuming that the synchrotron emitting region is a sphere with a radius of 3×10^{18} cm and that the energy densities of electron and magnetic fields are in equipartition (i.e., $u_e = u_B$). The model calculation code is adopted from Tashiro et al. (2009). In the calculation, we assume $u_e = u_B = 6.9 \times 10^{-11}$ erg/cm³ or 2.7×10^{-11} erg/cm³, corresponding to magnetic field strengths of $B \sim 42$ μ G or 25 μ G for $p = 2.5$ or 2.0 , respectively. Therefore, to account for the radio and X-ray luminosities, the maximum Lorentz factor for electrons, γ_{\max} , should be less than 10^7 , when p is larger than 2.0 . In other words, the maximum energy of accelerated electrons would be $E_{\max} \leq 10$ or 5 TeV for $p = 2.5$ or 2.0 , respectively, corresponding to a roll-off frequency of $\nu_{\text{roll}} \leq 10^{17}$ Hz.

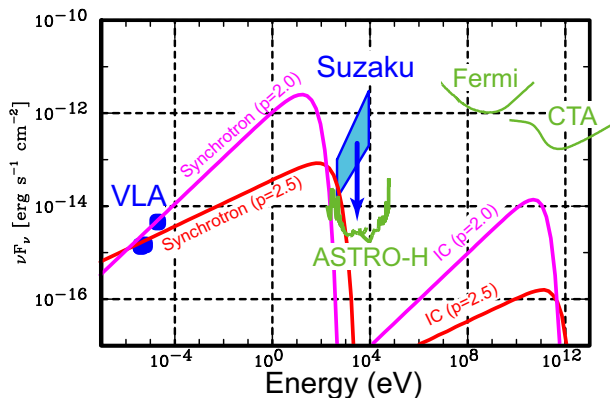


Fig. 3. The wide band energy spectrum of the shocked region of BD+43°3654 from the radio to the TeV band. The observation data from VLA and Suzaku are plotted in blue. The red and magenta lines show the energy distributions of synchrotron and inverse-Compton emissions from electrons with a Lorentz factor of 1 to 2.0×10^7 or 1 to 1.0×10^7 , and energy index $p = 2.5$ or 2.0 , respectively. In the calculation, we assume $u_e = u_B \sim 6.9 \times 10^{-11}$ erg/cm³ or 2.7×10^{-11} erg/cm³, ($B \sim 42$ μ G or 25 μ G) for $p = 2.5$ or 2.0 , respectively. CXB is only the source of inverse Compton emission in this calculation. The green lines show the sensitivities of the future X-ray mission *ASTRO-H* (Takahashi et al. 2010 and references therein), the Cherenkov Telescope Array (CTA) North, and the gamma-ray satellite *Fermi*.

Under the diffusive-shock-acceleration (DSA) theory (Bell 1978), particles need to be scattered back to the shock front multiple times, so magnetic-field turbulence in the upstream region of the shock is crucial for the DSA mechanism. Let us consider the time scales for the constraint of the magnetic-field turbulence, which is in the Bohm limit for PWNe and SNRs (c.f., Shibata et al. 2003; Bamba et al. 2003; Bamba et al. 2005). The cooling time scale of electrons with the maximum energy via synchrotron emission (~ 2.0 kyr and 4.1 kyr for $p = 2.5$ and 2.0 , respectively, from equation (2)) is longer than the dynamical timescale of ~ 1 kyr (see equation (3)). Thus

E_{\max} is determined from the balance of the acceleration and the dynamical timescales, and we obtain

$$\begin{aligned} E_{\max} &= \frac{3}{20} \frac{1}{\xi} \frac{v_s^2}{c} e B \tau_{\text{dy}} \\ &= \frac{60}{\xi} \left(\frac{v_s}{2300 \text{ km s}^{-1}} \right)^2 \\ &\quad \times \left(\frac{B}{25 \mu\text{G}} \right) \left(\frac{\tau_{\text{dy}}}{3 \times 10^{10} \text{ s}} \right) \text{ TeV}, \end{aligned} \quad (6)$$

where $\xi \sim (B/\delta B)^2$ is the ratio of the mean free path and the gyroradius of electrons (Skilling 1975; Jokipii 1987; Bamba et al. 2003; Nakamura 2010). In the Bohm limit, ξ becomes 1. Thus, the maximum energy should be $\sim 60/\xi$ or $108/\xi$ TeV, for $p=2.5$ ($B \sim 42$ μ G) and $p=2.0$ ($B \sim 25$ μ G), respectively. Observationally, these values should be less than 10 and 5 TeV, respectively, and so, in either case, we find that ξ should be larger than ~ 11 . Therefore, the magnetic field might not be as turbulent as in PWNe and SNRs.

Non thermal emission from protons, as well as electrons, could contribute possible Gamma-ray emission in Fermi and CTA band (Benaglia et al. 2010; del Valle & Romero 2012). The low level of turbulence from our results in the X-ray band with the assumption of equipartition between u_e and u_m indicates low acceleration efficiency, not only for electrons but also for protons. In this situation, the maximum energy of protons must be far below the knee energy of 10^{15} eV. Furthermore, if the magnetic-field turbulence is generated by accelerated protons themselves, as in the case of SNRs (Lucek & Bell 2000), the fact that $\xi > 11$ suggests a lower density of cosmic-ray protons in this system, which implies the proton injection rate is smaller than that in SNRs.

Acknowledgements

The authors would like to thank all the members of the Suzaku team for their continuous contributions in the maintenance of onboard instruments, spacecraft operation, calibrations, software development, and user support both in Japan and the United States. We would also like to thank the referee Dr. Andrei Bykov and the journal editor for careful readings and useful comments. This work was supported in part by Grants-in-Aid for Scientific Research (B) from the Ministry of Education, Culture, Sports, Science and Technology (MEXT) (No. 23340055, Y. T; No. 22340039, M.S. T), a Grant-in-Aid for Young Scientists (A) from MEXT (No. 22684012, A. B.), a Grant-in-Aid for Young Scientists (B) from MEXT (No. 21740184, R. Y.), and a Grant-in-Aid for Research Fellowship for Young Scientists (DC2) from the Japan Society for the Promotion of Science (No. 239311, T. K.). Finally, YT and AB would like to thank Saki Terada for continuous supports.

References

- Bamba, A., Yamazaki, R., Ueno, M., & Koyama, K. 2003, *ApJ*, 589, 827
- Bamba, A., Yamazaki, R., et al 2005, *ApJ*, 621, 793
- Benaglia, P., et al., 2010, *A&A*, 517, L10
- Bell, A. R., 1978, *MNRAS*, 182, 147
- Cassinelli, J. P. and Olson, G. L., 1979, *ApJ*, 229, 304
- Cheng, K. S. and Ho, C. and Ruderman, M., 1986a, *ApJ*, 300, 500
- Cheng, K. S. and Ho, C. and Ruderman, M., 1986b, *ApJ*, 300, 522
- Comerón, F., et al., 2002, *A&A*, 389, 874
- Comerón, F. and Pasquali, A., 2007, *A&A*, 467, L23
- del Valle, M., V. & Romero G., E., 2012, *A&A*, in press (arXiv:1204.4834)
- Fukazawa, Y., et al., 2009, *PASJ*, 61, 17
- Ginzburg, V. L., 1953, *Dokl. Akad. Nauk SSSR* 92, 1133
- Güdel, M., et al., 1997, *ApJ*, 483, 947
- Güdel, M., 2004, *A&A Rev.*, 12, 71
- Gvaramadze, V. V., and Bomans, D. J., 2008, *A&A*, 485, L29
- Hanson, M. M., 2003, *ApJ*, 597, 957
- Harding, A. K. and Gaisser, T. K., 1990, *ApJ*, 358, 561
- Ishisaki, Y., et al., 2007, *PASJ*, 59, S113
- Jokipii, J. R. 1987, *ApJ*, 313, 842
- Kaastra, J. S., Mewe, R., Nieuwenhuijzen, H. 1996, *The 11th Colloquium on UV and X-ray Spectroscopy of Astrophysical and Laboratory Plasmas*, 411
- Kalberla, P. M. W et al., 2005, *A&A*, 440, 775
- Kennel, C. F., & Coroniti, F. V. 1984, *ApJ*, 283, 694
- Kobulnicky, H. A., Gilbert, I. J., Kiminki, D. C., 2010, *ApJ*, 710, 549
- Koyama, K., et al., 1995, *Nature*, 378, 255
- Koyama, K., et al., 2007, *PASJ*, 59, S23
- Kushino, A., et al., 2002, *PASJ*, 54, 327
- Lagage, P. O. and Cesarsky, C. J., 1983, *A&A*, 118, 223
- Liedahl, Duane A., Osterheld, Albert L., Goldstein, William H., 1995, *ApJ*, 438, 115
- Lucek, S. G., & Bell, A. R. 2000, *MNRAS*, 314, 65
- Nakajima, H., et al., 2008, *PASJ*, 60, S1
- Nakamura, R., et al., 2012, *ApJ*, 746, 134
- Markova, N., et al., 2004, *A&A*, 413, 693
- Mewe, R., Gronenschild, E. H. B. M., van den Oord, G. H. J., 1985, *A&AS*, 62, 197
- Mitsuda, K., et al., 2007, *PASJ*, 59, S1
- Nazé, Y., et al., 2011, *ApJS*, 197, 7
- Ohashi, T., et al. 1996, *PASJ*, 48, 157
- Peri, C. S., Benaglia, P., et al., 2012, *A&A*, 538, A108
- Rees, M. J. and Gunn, J. E., 1974, *MNRAS*, 167, 1
- Reynolds, S. P. and Keohane, J. W., 1999, *ApJ*, 525, 368
- Repolust, T., Puls, J., & Herrero, A., *A&A*, 415, 349
- Ruderman, M. A. and Sutherland, P. G., 1975, *ApJ*, 196, 51
- Serlemitsos, P. J. et al., 2007, *PASJ*, 59, S9
- Shibata, S., Tomatsuri, H., Shimanuki, M., Saito, K., & Mori, K. 2003, *MNRAS*, 346, 841
- Shklovskii, I. S., 1953, *Dokl. Akad. Nauk SSSR* 91, 475
- Skilling, J. 1975, *MNRAS*, 172, 557
- Sturrock, P. A., 1971, *ApJ*, 164, 529
- Takahashi, T., et al., 2007, *PASJ*, 59, S35
- Takahashi, T., et al., 2010, *Proc. of SPIE*, 7732, 77320Z-77320Z-18
- Tashiro, M., et al., 2009, *PASJ*, 61, S327
- Tawa, N., et al., 2008, *PASJ*, 60, 11
- Terada, Y. et al. 2008, *PASJ*, 60, S25
- Terada, Y. et al. 2010, *ApJ*, 721, 1908
- Terada, Y., & Dotani, T., 2011, *the High-Energy Emission from Pulsars and their Systems* (editor: D. F. Torres and N. Rea, *Astrophysics and Space Science Proceedings*, ISSN:1570-6591), 563 (astroph/1006.5274)
- van Buren, D. and McCray, R., 1988, *ApJL*, 329, L93